Solid−Liquid−Vapor Phase Boundary of a North Sea Waxy Crude: Measurement and Modeling

Jean-Luc Daridon* and Jérôme Pauly

Laboratoire des Fluides Complexes - Groupe Haute Pression, Université de Pau, BP 1155, 64013 PAU Cedex, France

João A. P. Coutinho

Departamento de Química da Universidade de Aveiro, 3810 Aveiro, Portugal

François Montel

Total Fina ELF, CSTJF, Avenue Larribau, 64018 PAU, France

Received November 17, 2000. Revised Manuscript Received March 7, 2001

The wax appearance temperature as well as the liquid vapor phase boundary were measured on two condensate gases from a high-temperature−high-pressure field in the North Sea. Measurements were performed up to 45 MPa in the temperature range from 293 to 423 K. The experimental temperatures of wax appearance were then compared to the prediction of a model previously developed for synthetic light gas−heavy *n*-paraffins systems and adapted here to the representation of live oils.

Introduction

In deep fields, in which fluids are stored under high temperature and high pressure (HT-HP conditions), the light components in the supercritical state are able to dissolve a significant amount of heavy *n*-paraffins. These high-molecular-weight components which are soluble in crude oil under reservoir conditions may precipitate as a waxy solid phase due to a decrease in temperature or a change in composition of light components caused by gas-phase separations. In a cold environment such as that of the North Sea the cloud point temperature of the HT-HP fluids can be higher than ambient temperature and wax crystallization may occur in the off-shore production equipment. In particular, paraffins may deposit on the pipe wall when oil is transported through a long sub-sea pipeline or precipitate in the well when the flow is slow or during a prolonged interruption of the production. To evaluate the risk of wax deposition and to design techniques to prevent or to remove waxy solid deposits it is essential to be able to predict the conditions of appearance of waxes in live oils.

As the appearance of waxes is mainly caused by a decrease in temperature, most of the models have been designed to predict the wax appearance temperature and the influence of temperature on wax content of stock-tank oil[1−5] fuels[6−8] or synthetic mixtures[9,10] at atmospheric pressure. However, although it is less important, the pressure as well as the concentration of light gas components has a significant effect on the wax formation conditions.[11−14] To attempt to predict the solid−fluid equilibrium of light gases−heavy hydrocarbons systems under pressure, a model which relies on an equation of state−G^E model to describe the fluid phase behavior under pressure and based on a local composition concept to represent the solid-phase nonideality has been proposed in a previous paper.[15] The test of the procedure was only restricted to binary and ternary mixtures as well as multicomponent synthetic systems. To check the predictive capacity of this model for real HT-HP fluids, measurements of liquid−solid and liquid−vapor equilibria were carried out on two condensate gases from a North Sea reservoir in which

* Author to whom correspondence should be addressed.

(1) Won, K. W. *Fluid Phase Equilib.* **1986**, *30*, 265−279.
(2) Hansen, J. H.; Fredenslund, Aa.; Pedersen, K. S.; Rønningsen, H. P. *AIChE J.* **1988**, *12*, 1937−1942.
(3) Pedersen, K. S.; Skovborg, P.; Ronningsen, H. P. *Energy Fuels* **1991**, *5*, 924−932.
(4) Erickson, D. D.; Niesen, V. G.; Brown, T. S. *SPE* **1993**, 26604, 933−948.
(5) Lira-Galena,; Firoozabadi, A.; Prausnitz, J. M. *AIChE J.* **1996**, *42*, 239−248.
(6) Coutinho, J. A. P.; Ruffier-Meray, V. *Ind. Eng. Chem. Res.* **1997**, *36*, 4977−4983.
(7) Coutinho, J. A. P.; Dauphin, C.; Daridon, J. L. *Fuel* **2000**, *79*, 607−616.
(8) Coutinho, J. A. P. *Energy Fuels* **2000**, *14*, 625−631.
(9) Coutinho, J. A. P.; Andersen, S. I.; Stenby, E. H. *Fluid Phase Equilib.* **1995**, *103*, 23−29.
(10) Coutinho, J. A. P.; Knudsen, K.; Andersen, S. I.; Stenby, E. H. *Ind. Eng. Chem. Res.* **1996**, *35*, 918−925.
(11) Ruffier Meray, V.; Volle, J. L.; Schranz, C. J. P.; Le Marechal, P.; Behar, E. *SPE* **1993**, 26549.
(12) Pan, H.; Firoozabadi, A.; Fotland, P. *SPE Production Facilities*, Nov. 1993, 250.
(13) Brown, T. S.; Niesen, V. G.; Erickson, D. D. *SPE* **1994**, 28505, 415−430.
(14) Roenningsen, H. P.; Soemme, B. F.; Pedersen, K. S. Proceedings from Multiphase '97, BHR Group, 1997.
(15) Pauly, J.; Daridon, J. L.; Coutinho, J. A. P.; Lindeloff, N.; Andersen, S. I. *Fluid Phase Equilib.* **2000**, *167*, 145−159.

10.1021/ef000263e CCC: $20.00
Published on Web 04/28/2001

Table 1. Principal Characteristics of the Fluids

fluid characteristics	CG-A	CG-B
bottom hole pressure (MPa)	109	110
bottom hole temperature BHT (K)	454	459
saturation pressure at BHT (MPa)	34.2	33.9
molecular weight (g/mol)	37.8	37.0
total GOR at 15 °C (m^3/m^3)	854	906
C_{11}+ fraction (mol %)	4.88	4.30
molecular weight of C_{11}+ (g/mol)	234.9	237.5
heavier *n*-paraffin in C_{11}+	C_{32}	C_{35}
α	0.850	0.841
percentage of heavy *n*-paraffins in C11+	27.1	27.9
percentage of heavy *n*-paraffins in the fluid (mol %)	1.32	1.20

Table 2. Analytical Data of the Fluids

	CG-A		CG-B	
components	composition (mol %)	M_w (g mol^{-1})	composition (mol %)	M_w (g mol^{-1})
nitrogen	0.55	28.01	0.56	28.01
carbon dioxide	2.62	44.01	2.90	44.01
methane	68.44	16.04	69.13	16.04
ethane	8.98	30.07	8.16	30.07
propane	4.24	44.1	4.01	44.1
isobutane	0.80	58.12	0.87	58.12
n-butane	1.52	58.12	1.60	58.12
isopentane	0.68	71.92	0.83	71.92
n-pentane	0.66	72.15	0.74	72.15
C_6	1.39	84.93	1.52	84.95
C_7	1.71	97.82	1.76	97.81
C_8	1.50	111.51	1.56	111.5
C_9	1.12	126.14	1.13	126.12
C_{10}	0.91	139.15	0.91	139.99
C_{11}+ (*n*-paraffin)	1.32	228.60	1.20	229.04
C_{11}+ (non *n*-paraffin)	3.56	237.19	3.10	240.82

the bottom hole conditions correspond to a pressure higher than 100 MPa and a temperature higher than 450 K. Experimental results were then compared with those predicted by the model.

Experimental Section

Measurements were performed on two condensate gases, denoted CG-A and CG-B coming from various wells of a North Sea field. The first system comes from a reservoir 5300 m deep, whereas the sampling depth of the second is about 5700 m. Some of the bottom hole characteristics of these fluids are provided in Table 1. They are characterized by very high bottom hole temperatures and pressures, and are thus typical HT-HP fluids. The compositions of the fluids, which were determined by gas chromatography for the C_{20}-substances and permeable gel and gas chromatographic analysis for the C_{20}+ fraction, are summarized in Table 2 into 14 groups plus a heavy fraction (C_{11}+) which is split into the *n*-paraffins and the other components. The distribution of *n*-paraffins in the heavy fraction is detailed in Table 3. Examination of these tables reveals that both fluids are formed of more than 87% (in molar proportion) of light components (N_2, CO_2, and hydrocarbons up to C_4) whereas the C_{11}+ fraction represents less than 5% of the fluids. This quantity of heavy component of which one-third is *n*-paraffin is not negligible in comparison to the medium components (C_5 to C_{10}) which act as solvent of waxes at low pressure. Exploitation of such fluids therefore requires particular care, because when gas-phase separation occurs the proportion of *n*-paraffins in condensate may become significant and wax may appear. Compositional analysis of the C_{11}+ fraction shows (Figure 1) that the heavy *n*-paraffin are continually decreasing from C_{11} to C_{35} according to the recurrence relationship:

$$x_{c_{n+1}} = \alpha\, x_{c_n} \qquad (1)$$

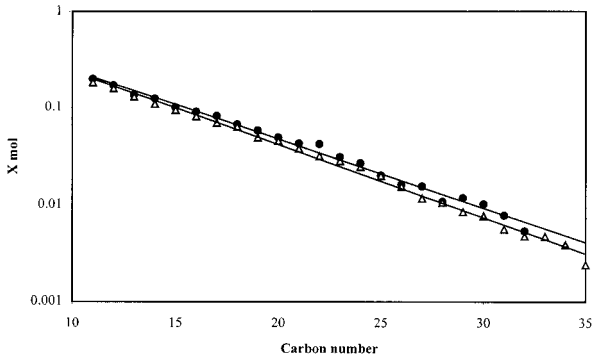

Figure 1. Composition of the heavy *n*-paraffins in fluids CG-A (●) and CG-B (△).

Table 3. Composition (mol %) of the *n*-Paraffins in the Fluids

paraffins	CG-A	CG-B
n-C_{11}	2.00×10^{-01}	1.83×10^{-01}
n-C_{12}	1.71×10^{-01}	1.59×10^{-01}
n-C_{13}	1.36×10^{-01}	1.30×10^{-01}
n-C_{14}	1.24×10^{-01}	1.09×10^{-01}
n-C_{15}	1.01×10^{-01}	9.41×10^{-02}
n-C_{16}	9.08×10^{-02}	8.12×10^{-02}
n-C_{17}	8.22×10^{-02}	6.95×10^{-02}
n-C_{18}	6.72×10^{-02}	6.36×10^{-02}
n-C_{19}	5.83×10^{-02}	4.94×10^{-02}
n-C_{20}	4.96×10^{-02}	4.56×10^{-02}
n-C_{21}	4.31×10^{-02}	3.82×10^{-02}
n-C_{22}	4.26×10^{-02}	3.19×10^{-02}
n-C_{23}	3.12×10^{-02}	2.85×10^{-02}
n-C_{24}	2.72×10^{-02}	2.48×10^{-02}
n-C_{25}	2.03×10^{-02}	2.00×10^{-02}
n-C_{26}	1.63×10^{-02}	1.56×10^{-02}
n-C_{27}	1.56×10^{-02}	1.17×10^{-02}
n-C_{28}	1.09×10^{-02}	1.07×10^{-02}
n-C_{29}	1.19×10^{-02}	8.52×10^{-03}
n-C_{30}	1.02×10^{-02}	8.52×10^{-03}
n-C_{31}	8.52×10^{-03}	8.52×10^{-03}
n-C_{32}	8.52×10^{-03}	8.52×10^{-03}
n-C_{33}		8.52×10^{-03}
n-C_{34}		8.52×10^{-03}
n-C_{35}		8.52×10^{-03}

in which α is equal to 0.85 which corresponds to the value normally encountered in waxy crude oils. Nevertheless, the distribution of heavy *n*-paraffin, which is generally continually decreasing up to C_{60} or $C_{80,}$ is for these HT-HP condensate gas cut down to C_{35}. This unexplained anomaly which does not come from the limits of the analytical technique may arise from the sampling procedure of reservoir fluids.

The onset crystallization conditions of waxy crudes are usually determined by indirect measurements such as flow properties (viscosimetry,[4] pressure drop across a filter[16]), differencial scanning calorimetry,[6,11,16] acoustic properties[11] (speed of sound and attenuation), and optical measurement (light transmittance,[17] cross polar microscopy[2,4,13,16,17]). However, as the fluids studied are quite transparent, the fluid−solid phase transitions were measured directly by visualization of the wax crystal appearance or disappearance using an all-round visibility setup. This experimental apparatus already used to measure liquid−solid equilibrium in synthetic systems[18] is made up of a sapphire autoclave cell housed in a glass casing within which a heat-conducting transparent oil bath circulates. The apparatus enables *PVT* analysis of samples of approximately 150 cm^3 volume, within pressure and temper-

(16) Monger-McClure, T. G.; Tackett, J. E.; Merrill, L. S. *SPE Production Facilities* **1999**, *14*, 4−16.
(17) Hammami, A.; Raines M. *SPE* **1997**, 38776, 273−287.
(18) Daridon, J. L.; Xans, P.; Montel, F. *Fluid Phase Equilib.* **1996**, *17*, 241−248.

Table 4. Wax Appearance Temperature Measured in Both Fluids

CG-A		CG-B	
T/K	*P*/MPa	*T*/K	*P*/MPa
285.95	40	295.15	40
285.65	39	294.45	35
285.55	38	293.55	30
285.25	37	292.75	25
284.85	36	292.95	20
285.39	35	291.75	15
285.53	34	290.15	10
285.85	33		
285.81	32		
285.01	31		
284.49	30		
283.85	25		
281.85	20		
280.05	15		
278.69	10		
278.61	8		
278.35	6		
278.19	4		

Table 5. Liquid−Vapor Phase Transitions Measured in Both Fluids

CG-A		CG-B	
T/K	P/MPa	T/K	P/MPa
374.03	34.86	423.32	33.43
363.15	34.73	413.45	33.59
352.37	34.63	403.15	33.74
343.23	34.46	393.25	33.82
333.43	34.22	383.65	33.78
322.95	33.9	373.75	33.74
313.75	33.56	364.15	33.63
303.57	33.19	353.65	33.48
292.91	32.79	343.85	33.32
283.43	32.26	333.15	32.99
278.43	31.7	323.55	32.8
		313.05	32.18
		303.25	31.75
		293.15	31.26

ature ranges of respectively 0.1−50 MPa and 273−423 K. Pressure is provided by a ROP brand volumetric pump and measured using an HBM P3M manometer. Temperature is measured using a platinum resistance inserted into the fluid.

Visual identification of appearance of the first crystal at constant pressure is particularly convenient in these condensate gases which are not too dark. Starting from a monophasic fluid phase or a liquid−vapor phase equilibrium state at the studied pressure, the system is slowly cooled (about 0.5 K per hour) and stirred until waxy solids appear. By this method the fluid−solid transition values are repeatable to within 1 K. Nevertheless, due to subcooling effects and size detection possibilities of eyes, measurements are checked by measuring the temperature of disappearance of the last crystal during an heating process. A deviation of 2 K was observed between these two different measurements. The cloud point temperatures were measured along isobars ranging from 40 to 4 MPa. The results are summarized for both systems in Table IV.

Using the same apparatus, the phase boundary between the homogeneous fluid phase and liquid−vapor region was also measured from the triple point to 423 K in order to characterize the full phase envelope of these fluids from the reservoir to the separator conditions. Vapor−liquid equilibrium data are listed in Table 5 and phase envelope of fluid CG-A is plotted in Figure 2. It can be seen on this figure that the increase of pressure tends to increase the melting temperature in the two-phase liquid−vapor region. This behavior means that the solubilization of light ends with pressure has less influence than the increase of fusion temperature of pure *n*-paraffins with pressure in the range of pressure investigated. The dissolution of light gas has a significant effect only between

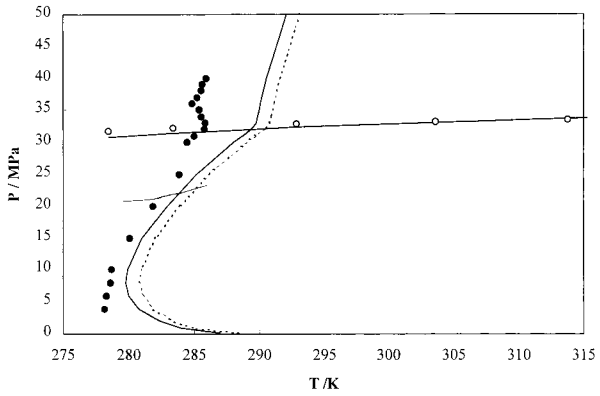

Figure 2. Measured and calculated phase boundaries in CG-A. ● Experimental fluid−solid transition points. ○ Experimental vapor−liquid transition points. - − - − Calculated points using Wilson, _ Calculated points using UNIQUAC.

atmospheric pressure to 5 MPa. It can be also observed on Figure 2 a change of the slope of liquid−solid line above the liquid−vapor phase boundary. To ensure that this unusual trend was not an artifact due to experimental uncertainties, the experimental pressure step was reduce and the number of experimental points was increase in this range of pressure for the fluid CG-A. This phenomenon, linked to an increase of the wax appearance temperature in the neighborhood of the bubble point, arises probably from the proximity of the critical point which has been estimated ranging between 310 and 360 K.

Model Predictions

The model used to predict fluid−solid-phase transition of these HT-HP fluids is a modification of the model proposed by Pauly et al.[15] for predicting solid−fluid and fluid−fluid phase equilibria of synthetic systems containing light gases and heavy paraffins under high pressure.

Fluid Phases Modeling. The behavior of the fluid phases is described using the Soave−Redlich−Kwong cubic equation of state[19] corrected by the volume translation of Peneloux:[20]

$$P = \frac{RT}{(V' - b)} - \frac{a}{V'(V' - b)} \qquad V = V' + C \quad (2)$$

where C is the translation parameter estimated at atmospheric pressure from a group contribution method.[20] However, to have a good description not only of fluid phase equilibrium, but also of the fugacity itself, the conventional mixing rule was replaced by the LCVM[21] mixing rule:

$$\alpha = \left(\frac{a}{bRT}\right) = \left(\frac{\lambda}{A_v} + \frac{1-\lambda}{A_m}\right)\left(\frac{G^E}{RT}\right) + \frac{1-\lambda}{A_m}\sum_i x_i \ln\left(\frac{b}{b_i}\right) + \sum_i x_i \alpha_i \quad (3)$$

in which $A_m = 0.64663$, $A_v = -0.693$, and $\lambda = 0.58$, and the excess Gibbs free energy G^E is calculated using the Modified UNIFAC group contribution method.[21]

(19) Soave, G. *Chem. Eng. Sci.* **1972**, *27*, 1197−1203.
(20) Peneloux, A.; Rauzy, E.; Frèze, R. *Fluid Phase Equilib.* **1982**, *8*, 7−23.
(21) Boukouvalas, C. J.; Spiliotis, N.; Coustikos, Ph.; Tzouvaras, N.; Tassios, D. P. *Fluid Phase Equilib.* **1994**, *92*, 75.

Waxy Solid-Phase Modeling. The waxy solid part is assumed formed of one or several orthorhombic solutions as have been observed experimentally.[22−23] The fugacity of a heavy *n*-paraffin in the solid phase is expressed as a function of pressure by the following relation:

$$x_i^{S}(P) = f_i^{S}(P_0)\exp\left\{\frac{1}{RT}\int_{P_0}^{P}\overline{V_i^{S}}\,dP\right\} \quad (4)$$

where $f_i^{S}(P_0)$ represents the solid fugacity at atmospheric pressure P_0, whereas the partial molar volume $\overline{V_i^{S}}$ is assumed proportional to the liquid molar volume:

$$\overline{V_i^{S_0}} = \bar{\beta} V_i^{L_0} \quad (5)$$

with β pressure independent. Thus, the integral of the partial molar volume is expanded in terms of pure liquid fugacity:

$$\frac{1}{RT}\int_{P_0}^{P}\overline{V_i^{S}}\,\frac{\bar{\beta}}{RT}\int_{P_0}^{P}\overline{V_i^{L_0}} = \ln\left(\frac{f_i^{L_0}(P)}{f_i^{L_0}(P_0)}\right)^{\bar{\beta}} \quad (6)$$

The solid fugacity at atmospheric pressure is evaluated in term of activity coefficient γ_i^{S}:

$$f_i^{S}(P_0) = x_i^{S}\,\gamma_i^{S}(P_0)\,f_i^{L_0}(P_0) \quad (7)$$

where $f_i^{S_0}$ is the fugacity of the pure solid which is related to the pure subcooled liquid fugacity $f_i^{L_0}(P_0)$ from the change of free energy between the pure solid and the liquid at temperature T. Assuming the heat capacity contribution of the Gibbs energy variation negligible, $f_i^{S_0}$ is expressed as a function of the melting temperature T^{m} and enthalpy ΔH^{m} as well as the solid−solid transition temperature and enthalpy T^{tr}, ΔH^{tr}:

$$f_i^{S_0}(P_0) = f_i^{L_0}(P_0)\exp\left\{-\frac{\Delta H^{m}}{RT}\left(1-\frac{T}{T^{m}}\right)-\frac{\Delta H^{tr}}{RT}\left(1-\frac{T}{T^{tr}}\right)\right\} \quad (8)$$

Thus, the fugacity of a *n*-paraffin *i* in the solid solution at a pressure *P* can be expressed only in terms of liquid fugacity and pure phase transition properties (T^{m}, T^{tr}, ΔH^{m}, ΔH^{tr}, $\bar{\beta}$) as well as the activity coefficient at atmospheric pressure:

$$f_i^{S}(P_0) = x_i^{S}\,\gamma_i^{S}(f_i^{L_0}(P_0))^{1-\bar{\beta}}\,(f_i^{L_0}(P_0))^{\bar{\beta}}\exp\left\{-\frac{\Delta H^{m}}{RT}\left(1-\frac{T}{T^{m}}\right)-\frac{\Delta H^{tr}}{RT}\left(1-\frac{T}{T^{tr}}\right)\right\} \quad (9)$$

The solid phase nonideality was originally described using the predictive Wilson equation which provides a good description of the phase behavior of waxy solutions. However, as the *n*-paraffin distribution is wide, solid phases splitting, which cannot be predicted by the Wilson equation, may occur[22,23] at temperature lower than the wax appearance temperature. To allow multi solid-phase equilibrium calculation, the UNIQUAC model[24] already used to predict wax appearance under atmospheric pressure,[25] was also considered for describing solid solution non-ideality. The version of the UNIQUAC model used is

$$\frac{G^{E}}{RT} = \sum_{i=1}^{n} x_i \ln\left(\frac{\Phi_i}{x_i}\right) + \frac{Z}{2}\sum_{i=1}^{n} q_i x_i \ln\frac{\theta_i}{\Phi_i} - \sum_{i=1}^{n} q_i x_i \ln\left[\sum_{i=1}^{n}\theta_j \exp\left(-\frac{\lambda_{ij}-\lambda_{ii}}{q_i RT}\right)\right] \quad (10)$$

with

$$\Phi_i = \frac{x_i r_i}{\sum_j x_j r_j} \text{ and } \theta_i = \frac{x_i q_i}{\sum_j x_j q_j} \quad (11)$$

and using structural parameters *r* and *q* estimated[25] to take into account the specificity of the interactions in the solid phase:

$$r_i = \frac{r_{iorg}}{6.744} \text{ and } q_i = \frac{q_{iorg}}{5.40} \quad (12)$$

The pair interaction energy λ_{ij}, which is related to the contact area between the molecules *i* and *j*, is assumed[10] identical to the contact area between two molecules *j* which is the *n*-alkane with the shorter chain. This pair interaction energy is estimated from the heat of sublimation of an orthorhombic crystal of the pure component:

$$\lambda_{ij} = \lambda_{jj} = \frac{1}{3}(RT - \Delta H_j^{Sub}) \quad (13)$$

where the heat of sublimation is calculated at the melting temperature of pure components from the heat of vaporization melting and solid−solid transition:

$$\Delta H_j^{Sub} = \Delta H_j^{vap} + \Delta H_j^{m} + \Delta H_j^{tr} \quad (14)$$

The Solid−Liquid equilibrium model is thus a purely predictive model related only to pure component properties:

- T^{m}, T^{tr}, ΔH^{m}, ΔH^{tr}, determined for both even and odd *n*-paraffins from a correlation of the values of Broadhurst[26] for the odd *n*-paraffins.
- ΔH^{vap} calculated using the correlation proposed by Morgan and Kobayashi.[27]
- β estimated to 0.86 for pure components from the average of the solid−liquid volume change measured by Shaerer et al.,[28] whereas for mixtures of *n*-paraffins ranging from C_{20} to C_{40}, $\bar{\beta}$ is evaluated from measurements of Chevallier et al.[29] to 0.90 in order to take into account the excess volumes.

(22) Craig, S. R.; Hastie, G. P.; Roberts, K. J.; Gerson, A. R.; Sherwood, J. N.; Tack, R. D. *J. Mater. Chem.* **1998**, *8*, 859−869.
(23) Chevallier, V.; Briard, A. J.; Petitjean, D.; Hubert, N.; Bouroukba, M.; Dirand, M. *Mol. Cryst. Liq. Cryst.*, in press.
(24) Abrams, D. S.; Prausnitz, J. M. *AIChE J.* **1975**, *21*, 116−128.
(25) Coutinho, J. A. P. *Ind. Eng. Chem. Res.* **1998**, *37*, 4870−4875.
(26) Broadhurst, M. G. *J. Res. Nat. Bur. Stand.* **1962**, *66A*, 241−249.
(27) Morgan, D. L.; Kobayashi, R. *Fluid Phase Equilib.* **1994**, *94*, 51−87.
(28) Schaerer, A. A.; Busso, C. J.; Smith, A. E.; Skinner, L. B. *J. Am. Chem. Soc.* **1955**, *77*, 2017−2018.
(29) Chevallier, V.; Provost, E.; Bourdet, J. B.; Bouroukba, M.; Petitjean, D.; Dirand, M. *Polymer* **1999**, *40*, 2121−2128.

Lumping Procedure. The representation of petroleum fluids used in Total Fina Elf was adopted. It consists of separating the fluid into a light fraction which covers carbon dioxide, nitrogen, and hydrocarbons with less than 11 carbon ($C_{11}-$) and a heavy fraction ($C_{11}+$). The light fraction, whose composition is completely known and for which all the critical properties of the components are available,[30] is broken down into 14 cuts to simplify the representation of the fluid.[31] Each cut is either a pure component (up to C_5) or a pseudo-component which groups together all the molecules comprising the same number of carbon atoms.

The heavy fraction, usually considered as a single pseudo-component, must be, for waxy solid deposit calculation, split into the *n*-paraffin cut and the non *n*-paraffin cut in order to differentiate between components able to precipitate and those which cannot precipitate. The non *n*-paraffin cut includes the heavy iso paraffins, aromatics, and naphthenics components in a single pseudo-component and no attempt was made to draw a distinction between these chemicals families. A hypothetical molecule, made of CH_3, CH_2, and CH groups, is defined with the same molar mass as the heavy non *n*-paraffin cut in order to estimate the UNIFAC parameters. The pseudo-critical properties T_c, P_c, ω of the heavy cut are first estimated by means of group contribution methods[32−34] and then tuned in order to fit the liquid−vapor phase boundary curves. Contrary to the non *n*-paraffin components, heavy normal paraffins cannot be grouped in a single pseudo-paraffin with an average property of the distribution since the melting temperature of *n*-paraffin increases exponentially with increasing carbon number and thus the wax appearance temperature is principally affected by the shape of the distribution of heavy *n*-paraffins in the $C_{11}+$ fraction. Consequently, the $C_{11}+$ *n*-paraffin part is be described by the detailed composition of *n*-paraffins from C_{11} to the heaviest one. The Twu correlation[34] was used to predict their critical properties.

Results and Discussion

The critical parameters of the non *n*-paraffin $C_{11}+$ fraction were first tuned to provide a good description of the liquid−vapor phase boundary curve. Afterward fluid−solid transition curves were predicted without any fitting parameters. The calculation results along with the experimental wax appearance temperature of the cloud points data are plotted on Figure 2 for the condensate gas A. It can be observed, above all, that the model introduces only a slight shift of the wax appearance curves along temperature axis. The calculated wax appearance temperatures are overestimated by about 4 K using the Wilson equation and 3 K with UNIQUAC which is very close to the experimental uncertainty link to subcooling effects. Although UNIQUAC predict only one solid phase at the onset of crystallization like the Wilson equation does, using UNIQUAC instead of the Wilson equation leads to a translation of the wax appearance curve along the temperature axis. This translation provides a slight improvements of the predictions. The results of the comparison between experimental phase equilibrium data and the values supplied by the model using UNIQUAC are summarized for both fluids in Figure 3. It can be noticed on this figure that the model provides a good estimation of the change of wax appearance temperature caused by a small change of composition link to the difference of the deepest well in the same field. The results obtained for the second condensate gas are similar to those obtained with CGA with an average deviation of about 2.5 K.

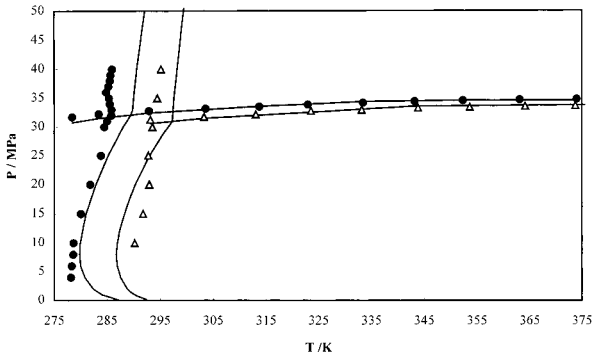

Figure 3. Comparison of predictions of the model using UNIQUAC and experimental phase envelopes for both fluids. ● Experimental data for CG-A. Δ Experimental data for CG-B. _ Predictions of the model using UNIQUAC.

Examination of these comparative tests reveals non systematic degradation when one moves from synthetic systems, (tested by Pauly et al.[15]) for which the feed composition of both heavy *n*-paraffins and solvent is well-known, to complex systems whose composition is lumped. These results show that the loss of information on the exact composition of the solvent part does not generate major changes in the predictive capacity of wax appearance temperature. A good description of the distribution of *n*-paraffins in the heavy fraction seems to be essential for predicting the wax appearance temperature of crude oils. The lumping into 15 cuts associated with a full description of the composition of high-molecular-weight *n*-paraffins appears to be well adapted to the prediction of the onset of wax crystallization situation, combining both simplicity of numerical processing and effectiveness. Thus, the analytical description of heavy *n*-paraffins, which can be obtained easily by gas chromatography, should be considered as the minimum information required for the characterization of fluids which may cause solid deposition difficulties during the exploitation or the transportation throw pipelines.

For both fluids studied here the distribution of heavy *n*-paraffins is broken down around C_{32} and C_{35}, while wax present in petroleum crudes generally contains *n*-paraffins up to C_{60}. If this break in the distribution of heavy *n*-paraffins comes from the procedure of sampling of the live oil, the mixtures studied do not correspond exactly to the reservoir fluid and the physical properties of the sample may be different than those of the reservoir fluid. To study the impact of the heavy ends on the solid−fluid equilibrium properties of the fluid, the distribution of the heavy *n*-paraffins was extended to the C_{60} using the recurrence relationship

(30) Reid, R. C.; Prausnitz, J. M.; Poling B. E. *The properties of gases and liquids*, 4th ed.; McGraw-Hill: New York, 1987.
(31) Montel, F.; Gouel, P. *SPE* **1984**, 13119, 16−19.
(32) Fedors, R. F. *Chem. Eng. Commun.* **1982**, *16*, 149−157.
(33) Nath, J. *Ind. Eng. Chem. Fundam.* **1983**, *22*, 325−326.
(34) Twu, C. H. *Fluid Phase Equilib.* **1984**, *16*, 137−150.

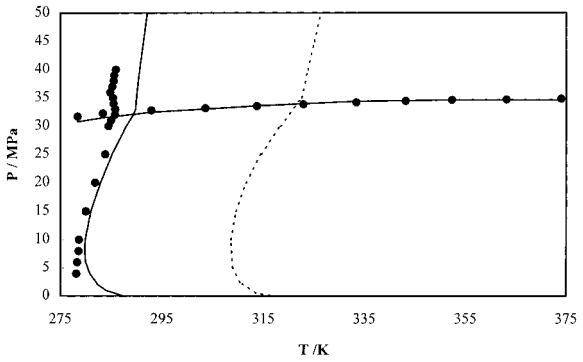

Figure 4. Comparison of wax appearance temperatures calculated using UNIQUAC with the heavy *n*-paraffin distribution cut down to C_{32} (——) and extrapolated to C_{60} (- − - − -). ○: Experimental data.

(1) with α determined from the *n*-paraffins ranging from C_{15} to C_{30}. This extrapolation out to C_{60} leads to an increase of the heavy *n*-paraffin in the fluid of 0.04% and moves the average molar mass of the *n*-paraffin distribution from 222 to 236 g mol^{-1}. The cloud points calculated by the model with this modified composition were compared with those predicted for the real composition system in Figure 4. It can be noted from this figure that the cloud point values are significantly higher for the extended *n*-paraffin distribution. The wax appearance temperatures are translated of about 30 K despite the small amount of heavy component added (about 2.5% of the distribution). This situation confirms that the full composition of the heavy *n*-paraffins, has to be taken into account to model the onset of wax crystallization.

Nomenclature

A = mixing rule parameter
a,b,C = equation of state parameters
f = fugacity
G = Gibbs free eneregy
H = enthalpy
P = pressure
q = area parameter (UNIQUAC)
R = ideal gas constant
r = volume parameter (UNIQUAC)
T = temperature
V = volume
x_i = mole fraction of i
Z = coordination number

Greek letters

α = distribution coefficient or a/(bRT)
β = volume change parameter
γ = activity coefficient
λ = parameter of LCVM or interaction parameters of UNIQUAC OR Wilson equation
ϕ = volume fraction
θ = area fraction

Superscripts

E = Excess
L = liquid
m = melting
S = solid
sub = sublimation
tr = solid−solid transition
vap = vaporization
V = vapor
‘ = Properties calculated from the SRK equation of state
_ = Partial property

Subscripts

i = component
0 = pure component or atmospheric

EF000263E